On the deconvolution of Unidentified Extended Objects from the Planetary Nebula Spectrograph

Johan Hidding, Groningen University, Kapteyn institute
Supervisors: Nigel Douglas and Saleem Zaroubi

March 11, 2009

1 Abstract

This project is centered around a typical problem in astronomy with an atypical instrument, the Planetary Nebula Spectrograph (PN.S). The PN.S has produced some exciting results regarding the dark matter content of *early* type galaxies. These results however are not without controversy. It is therefore important to know about any residual effects that would influence the confidence level of these results.
As Douglas et al. (2007) mentions, there is contamination from non-PNe objects. These are objects that are slightly more extended than the PSF and must be rejected as possible PNe. It is interesting to see what else they might be, because versions smaller than the PSF might contaminate the PN.S images unnoticed. To learn more about these objects, the goal of this project was to try and deconvolve these "unidentified extended objects". Despite the inherently small amount of data, we will show that using a simplified model we can in fact recover some information from the data. This is achieved using a model of an object with a rotational velocity structure and fitting it to the data using a least squares method.

2 Planetary Nebula Spectrograph

2.1 Studying extragalactic planetary nebulae

In the tireless pursuit for evidence of dark matter, astronomers have used many different tracers of the dynamical mass of a galaxy. The dynamics of spirals has been intensively studied by their HI gas content. But with ellipticals this is not so easy. There is (almost) no gas in these systems. Also the dynamics is more thermal having little bulk motion. It is near impossible to resolve individual stars at these distances. That is why some have resorted to study planetary nebulae to trace the dynamics of ellipticals. There are several reasons for this.

- PNe are prominent by their strong 500.7 nm OIII emission line.
- PNe are detectable up to large radii.
- PNe are a representative subset of the stellar component.

Now comes the task of detecting PNe in the system of study, and find the redshift of each of them. Traditionally this is done in a very time consuming way. The observer first has to make two images of the system; one in a broad band, the other in a narrow band OIII filter. From these one can select candidate objects and do follow up spectrography on each object. Theoretically this could also be done using Fabry-Perot spectrography, but there are several practical limitations to this. These techniques are very expensive in terms of telescope time, and the noise is really hard to deal with.

2.2 In comes the PN.S

This is why the PN.S group invested time and money to build an instrument specifically geared to observing extragalactic PNe by a technique called counter dispersive imaging or CDI. It allows to do these observations in one shot with high efficiency.

2.3 The instrument

The PN.S makes two slitless spectrum images simultaneously, with opposite dispersion directions. A line-emitter with some redshift due to its radial velocity will be shifted to the right on the one image, and to the left on the other.
Incoming light is filtered on the OIII line and then put through a slitless spectrograph. PNe have strong narrow line emission in OIII, so they show up as dots, while continuum objects will show bars following the filter profile. To measure the position and the redshift of the PNe at the same time another spectrum is made with opposite dispersion direction. If we then compare the two images, the dots will be offset from each other by an amount twice their velocity (with respect to the calibrated zero-velocity). The real position of the nebula will be just in between the dots on the two images.

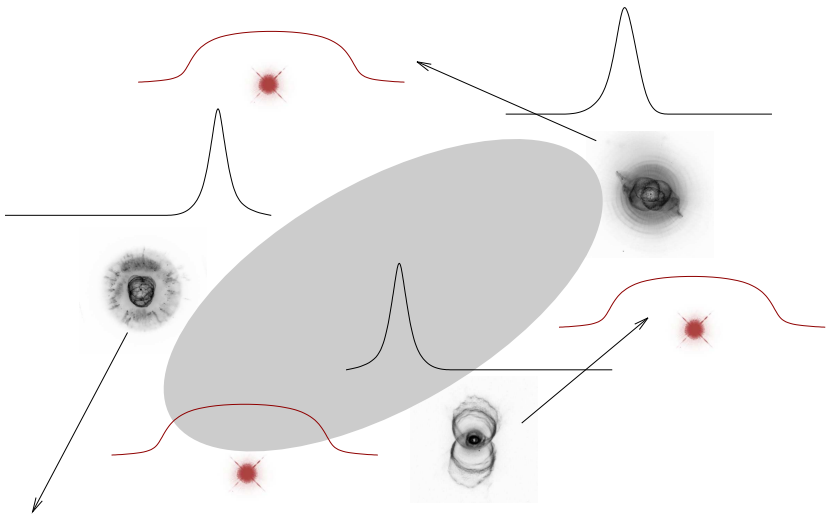

Figure 1: The scene of investigation. Shown on this diagram is the host galaxy with some of its PNe with different redshifts. Also there are foreground stars. On top of the objects is a spectrum each would give. The foreground stars just show the narrow band filter profile.

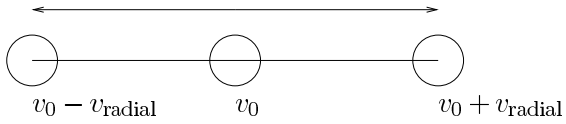

2.4 Science with the PN.S

In a paper by Romanowsky et al. (2003)[1] the results results of the PN.S observation of NGC 3379 were published. The dark matter content of the system turned out to be much lower than predicted by current cosmological ΛCDM models. This could be a big problem for galaxy formation theories.
Dekel et al. (2005)[2] showed that the apparent lack of DM can be explained by very elongated stellar orbits after disk-galaxy mergers. These orbits combined with projection effects will result in PNe having very small velocities in the line of sight. They predict that "σ_{p} (projected radial velocity dispersion) flattens toward $\sim 10R_{\text{eff}}$" while the "'naked' model predicts a continuing decline beyond $3R_{\text{eff}}$". The PN.S team claims [3] these projection effects are still not enough to allow for "conventional" mass to light ratios. The *real* observations simply disagree with the numerical models. The argument goes on at a level of "the observers' kinetic modelling is wrong" and "'observations' from numerical simulations don't tell you anything". Time will tell.

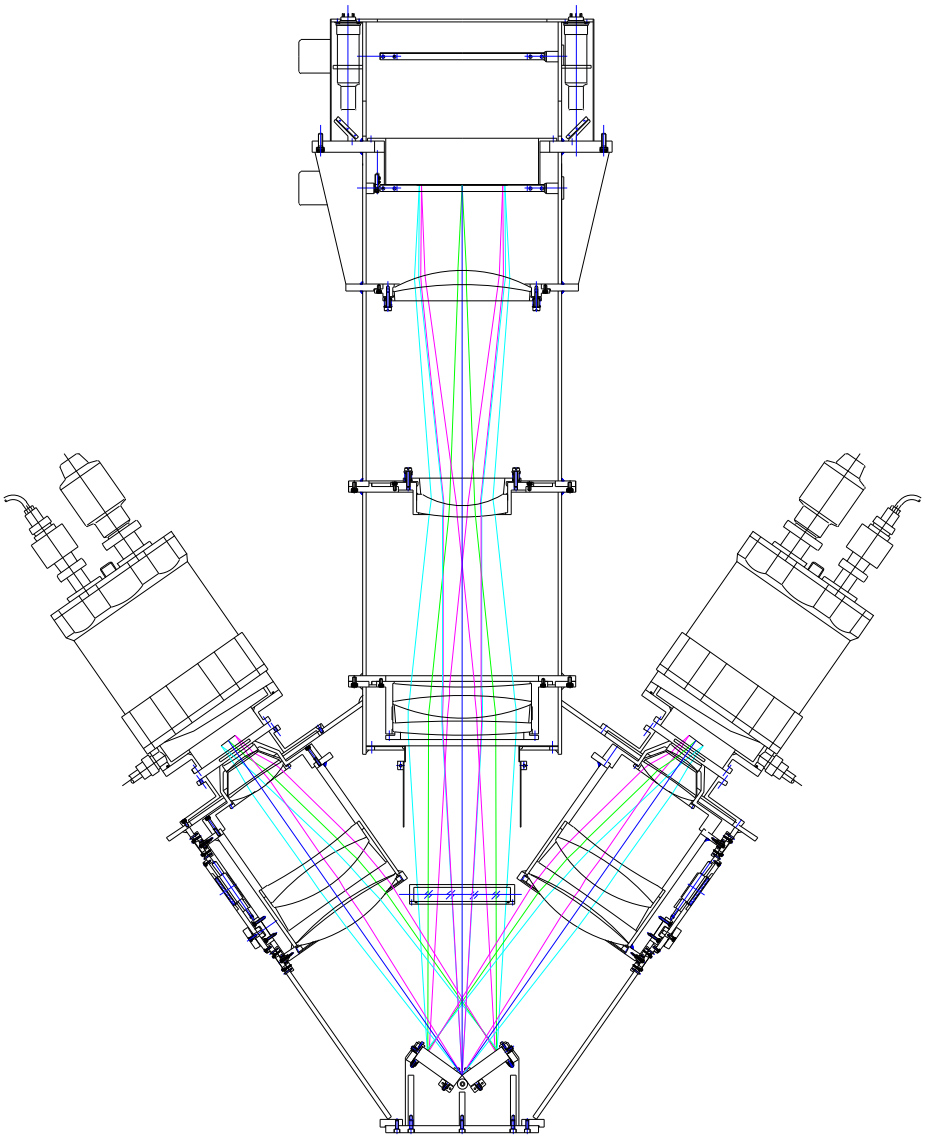

Figure 2: PN.S instrument design. In this image we can see the light travel from the telescope's focal point. First the beam is collumnated. Then at the bottom of the instrument are located two gratings which have opposite dispersion direction by their orientation to the beam. These also act as beam splitter. Then each arm brings its beam back into focus onto the two CCDs.

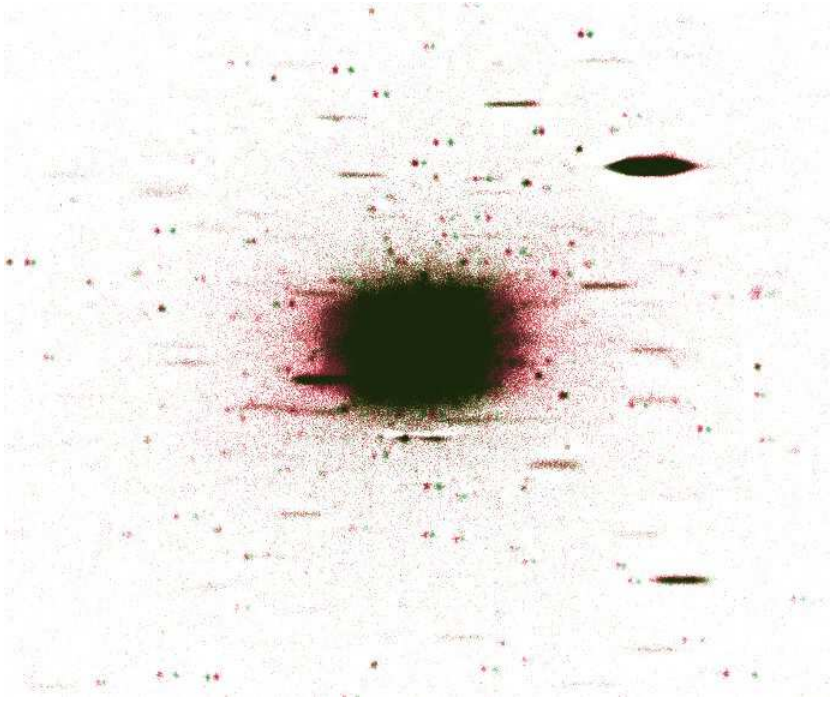

Figure 3: Composite PN.S image of NGC 3379. The planetary nebulae show up as dots, the bright bars are foreground stars. The two images were median subtracted using IRAF and combined using the GIMP. The green colour represents the image from the left arm, while red shows the right arm image.

2.5 This project

The data gathered with the PNS might be contaminated. There are several objects on the images that are slightly larger than the PSF. These unidentified extended objects might be galaxies at a large redshift. For example a galaxy with strong emission in OII (372.7 nm) would appear on the image if it were at redshift $z = 0.34$. The image of such a galaxy would be distorted to a fair amount by the spectrograph. The goal of this project is to model the way the spectrograph convolves the galaxy's image, and then to try to fit a simple model of a galaxy to some real data.

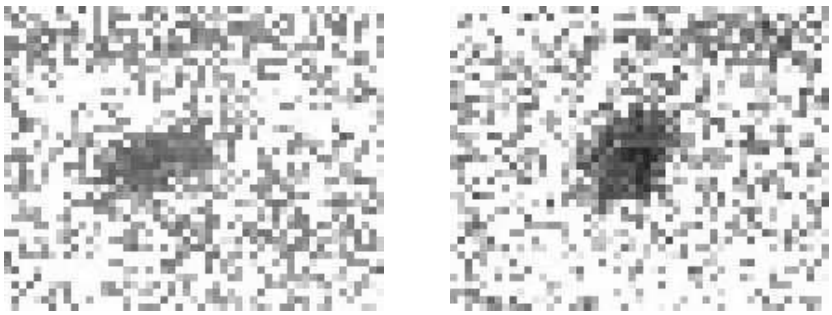

Figure 4: Detail from the NGC 3379 image. We observe two ellipsoids of different shape, clearly larger than the point spread function. There are a dozen similar occurrences in the entire image.

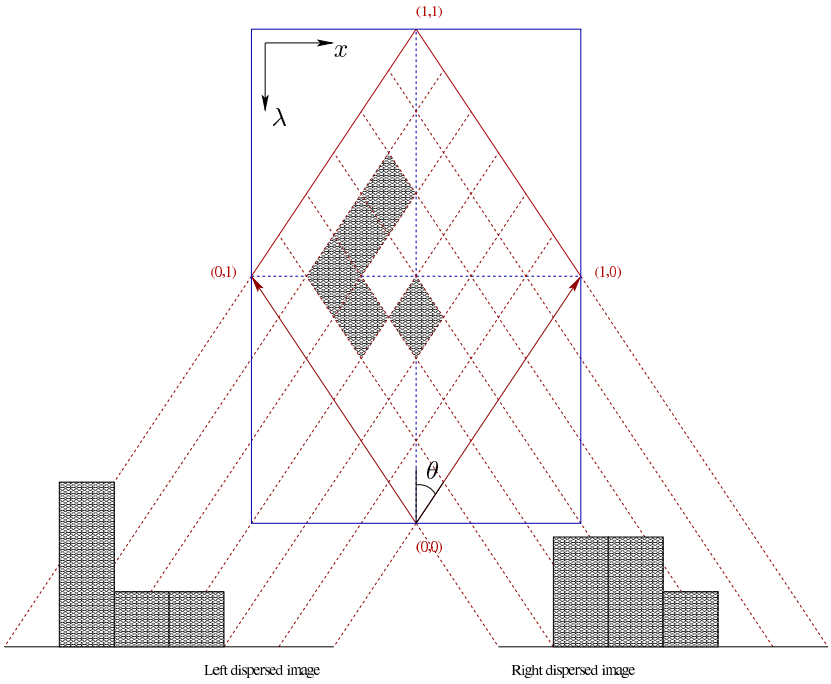

Figure 5: Illustration of the two projections the PN.S makes of one line on the image. Even this simple example using artificial data already has multiple solutions.

3 Convolution

From now on, we will treat the PN.S as an instrument making two different projections of the same $xy\lambda$ data cube. The big problem with deconvolving the data is that it is heavily degenerate. We humans can see depth because we get two projections of an optically thick object from slightly different perspectives. However if we were to look through an optically thin medium our ability to see the structure of this medium in three dimensions would vaporise like the mist it is made of. To give another approach, in souvenir shops you can buy paperweights with a three dimensional bubble sculpture inside (of the Eiffel-tower or the Colosseum). If you want to see the complete structure of the object, you need to turn the cube back and forth. Even with two eyes our vision is basically two dimensional.

3.1 Projection

Making a projection of a three dimensional object is done by the Radon transform

$$\mathcal{R}(r,\alpha)[f(x,y)] = \int_{-\infty}^{\infty}\int_{-\infty}^{\infty} f(x,y)\delta(r - x\cos\alpha - y\sin\alpha)\mathrm{d}x\mathrm{d}y$$

This transformation can be extended to higher dimensions. This is just a complicated way of saying that we integrate an object over the line of sight at angle α.

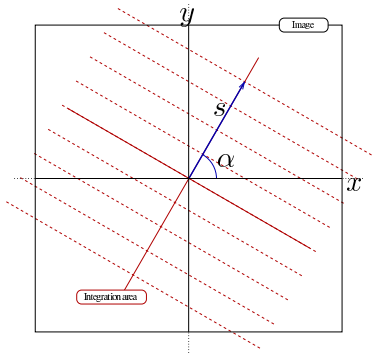

Figure 6: The Radon transform.

To invert this transformation, we need to apply the Fourier projection-slice theorem.

3.2 Fourier projection-slice theorem

The Fourier transform of the projection of an image is equal to a slice from the 2D Fourier transform of the entire image. In theory to completely and unambiguously reconstruct the image from a set of projections, we need an infinite amount of projections from different angles. Only then, will we have a complete coverage of the Fourier space. This technique is called tomographic reconstruction. In reality we never have an infinite amount of projections, so there will be gaps in Fourier space. There are many ways to fill these gaps. The idea is illustrated in fig 7.
Here's a proof of the Fourier slicing theorem (from Wikipedia).

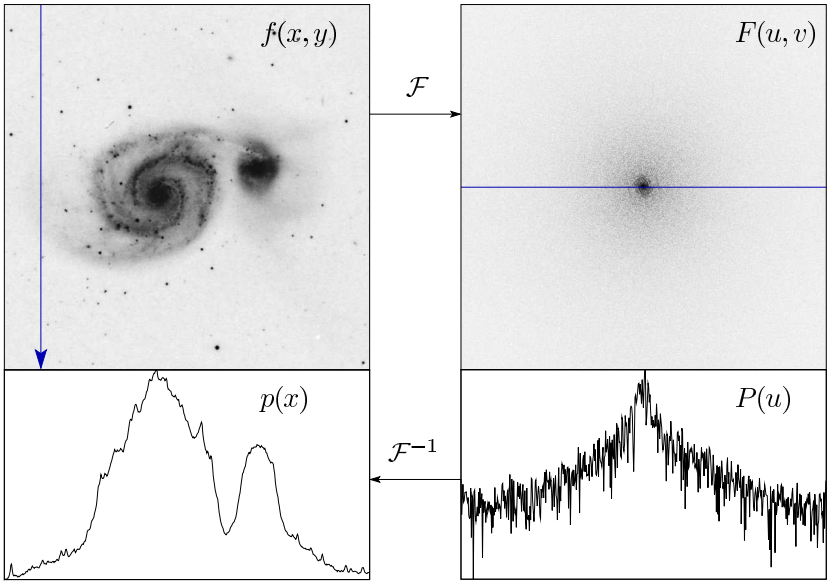

Figure 7: Illustration of the Fourier projection method. On the top left is a picture of the Whirlpool galaxy (taken from DSS using Skyview [http://skyview.gsfc.nasa.gov/]). This image is transformed using a two-dimensional Fourier transform to the image on the right. A slice is taken from the transformed image which is shown at the bottom right. This slice is then inverse transformed to the final result, which is equal to the first image integrated downwards.

$$
\begin{aligned}
p(x) &= \int_{-\infty}^{\infty} f(x,y)\mathrm{d}y \\
F(u,v) &= \int_{-\infty}^{\infty}\int_{-\infty}^{\infty} f(x,y)e^{2\pi i(ux+vy)}\mathrm{d}x\mathrm{d}y \\
P(u) &= F(u,0) \\
&= \int_{-\infty}^{\infty}\int_{-\infty}^{\infty} f(x,y)e^{2\pi iux}\mathrm{d}x\mathrm{d}y \\
&= \int_{-\infty}^{\infty}\left(\int_{-\infty}^{\infty} f(x,y)\mathrm{d}y\right)e^{2\pi iux}\mathrm{d}x \\
&= \mathcal{F}(p(x))
\end{aligned}
$$

3.3 Degeneracies in tomography

The projection-slice theorem only works with an infinite number of projections. Whenever there is a finite number of projections degeneracy will occur. To

lift the degeneracies we need to fill the gaps in the Fourier space. There is an entire body of literature on ways to achieve this. To do this when we have only two projections available verges on the impossible. This means that complete deconvolution of PN.S data is impossible.

4 Deconvolution

The PN.S is a slitless spectrograph. This gives rise to a degeneracy in the images. There is nothing telling us whether some bit of flux is emitted by one object on some frequency, or by some other on another frequency. This is the reason why the PN.S has *two* gratings, dispersing in opposite direction. The light is first filtered using a narrow band filter which covers the 500.7 nm line (shifted by the redshift of the host galaxy). The PNe then show up as single line emitters. The objects of our study however have an internal velocity structure as well as a spacial structure; which we know because the object has different shapes on the two images.

4.1 Deconvolution methods

The problem with deconvolution is that there is not one single solution. There's a range from which we need to choose the most probable one. This makes our task two-sided. We need to define a few criteria that we'd like the solution to adhere to. Then we need to find an algorithm that gives us this solution.

4.2 MOSES (the Multi-Order Slitless EUV Spectrograph) method

This method uses the property that flux is always a positive real number. All values in the resulting data cube need to be real and positive. It goes through a cycle which, if it converges, returns data which in Fourier domain fits the desired diagonal projections and in Cartesian domain is positive real everywhere.

1. Plot transforms of the projections onto Fourier space
2. Invert Fourier space to create the image
3. If the image is positive real everywhere, we're done
4. Otherwise take the real part and crop negative values
5. Transform to Fourier space
6. return to step 1

This cycle can be extended with any number of constraints to enhance the final image. We could for example assume the objects are emitting in one line only. So there should be only one maximum in the λ direction. Also we should take care the flux is conserved. In the case of the PN.S this is a hopeless approach as there are not enough projections available to do full deconvolution.

4.3 "Japanese Puzzle" Method

This idea is inspired on the Japanese image puzzles where you get a grid of pixels which can either be black or white. To solve it you need to use numbers which say how many pixels are consecutively black in each row and column.
The projections of the test images have large areas where they are zero. This means large areas on the $x\lambda$ plane are zero for sure. Then the rest of the image can be of some higher value that adds up to the threshold value h. Then the projections of this first image can be subtracted from the original projections and the procedure repeats.
If the image has large contrasts, the method can be sped up by starting with a large threshold, decreasing it each step, progressing to greater detail.
We implemented a simple version of this algorithm using two projections, it returns valid solutions, and we are confident that this method also works when there are more projections available.
Still, the returned solution will not be unique unless we have an infinite amount of projections.

4.4 Least-squares fitting using a parametric model

The previous two methods only do complete deconvolution and are therefore not suited to solve the problem with the PN.S images.
With complete deconvolution being such a hopeless case, we need to use a parametric fit. With only a few parameters we can make something that looks a bit like galaxy in $xy\lambda$-space, in our case this will be an ellipsoid with a certain inclination due to its solid-body rotation.
Given that the extended objects on the image are all more or less elliptical, this is not such a bad approach.

5 Least squares fitting

5.1 Modelling the object

To model the object we use an ellipsoid with a Gaussian profile.

$$D(x,y,\lambda;I,r,q,s,\phi,\sigma) = \frac{I}{(2\pi)^{3/2}r^2\sigma}\exp\left[-\frac{1}{2r^2}\left(u^2q+\frac{v^2}{q}\right)-\frac{1}{2\sigma^2}(s\ u-\lambda)^2\right]$$

where $u = x\cos\phi - y\sin\phi$ and $v = x\sin\phi + y\cos\phi$ and

I Total flux.

r Average radius in pixels.

q Ellipticity. This should be a number in $< 0, 1]$. A value of 1 gives an object with circular form, 0 a line. The parameter is constructed such that it has no influence on the total area of the ellipse.

s Rotation velocity times dispersion, in units of pixel per pixel. This is a purely mathematical parameter, which is explained further on.

ϕ The angle of the rotation. We consider only the radial component.

σ Width of the emission line.

This model is far from perfect. Galaxies generally don't follow a Gaussian profile, the way the model rotates as a solid body is not realistic either. However it is very simple, and produces results that are quite close to real images. The reasons why this model is a reasonable approximation are the following:

- The objects are not much bigger than the PSF. This means the Gaussian profile might not be so bad after all.
- We know all the derivatives of the function analytically.
- It represents a simple object with a simple velocity structure.
- The output is a set of elliptic objects, which is what the images look like.

5.2 Modelling the PN.S

Let $D(x,y,\lambda)$ be the original data cube.

$$I_L(x,y) = \int D(x+\delta\lambda, y, \lambda)d\lambda$$

$$I_R(x,y) = \int D(x-\delta\lambda, y, \lambda)d\lambda$$

I_L and I_R now represent the data received from the instrument. The dispersion of the PN.S is 1.29Å per pixel. This means that the shift of one pixel is roughly $1.29/5007\times c \approx 77$km/s. For comparison the rotation velocity of the Sun around the centre of the Galaxy is $220km/s$.

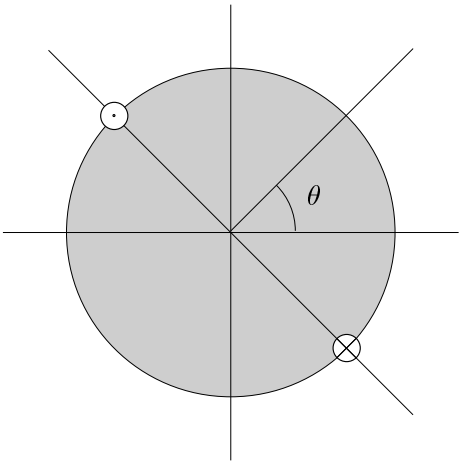

Figure 8: The simplified model of an object with some velocity structure

5.3 Testing the model

To test the LSF method, we first generate a few sample images, using the same functions that are used to fit them to, and then add some noise. Then we try to recover the input parameters from the two "PN.S images". If there are any degeneracies left in the process they should show up on the χ^2 map of the parameter space.
We will fix all but two parameters to the input value of the model. Then run a χ^2 test on the models that are created from the space of the remaining two parameters. For each input model this will generate a map that shows the goodness-of-fit for the entire parameter space. If there are degeneracies left these will show up on these maps.
Note that this is only a mathematical test. There is no input from outside. The measure of rotation velocity is in units of pixels dispersion per pixel on the line of rotation. If the studied object would be a straight vertical line the velocity is the tangent of the angle of the line to the vertical on the image.
If an object would be 10 pixels wide (a 5 pixel radius), and we take $s = 2$. On the modelled PN.S image it would have a shift of 10 pixels at the outer edges. This would imply a physical rotation velocity of 770km/s. If we compare this with the velocity of the Sun, it is a bit high, but on the same order of magnitude. Also note that when images get smaller, relative distortions get bigger.
To simplify further, we make this test only on circular objects, so q is fixed to a value of 1. With this model 25 different objects are created with θ being $0, 1/6\ \pi, 1/4\ \pi, 1/3\ \pi$ or $1/2\ \pi$ and the velocity going from 0 no rotation to 2 fast rotation. Of these models the PN.S would generate 50 images.

5.4 χ^2 distribution

To do the least squares fitting, we need to calculate the χ^2 first. In the simulated images we added a constant Gaussian noise that made the images similar to the samples of real data. This causes the first uncertainty to the contour levels we calculate. Our χ^2 is calculated thus:

$$\chi^2 = \frac{1}{N} \sum \frac{(y_i - y(x_i))^2}{\sigma^2}$$

where y_i is the simulated data at pixel i and $y(x_i)$ is the value of the model at the same pixel, σ is the amount of added noise and N is the amount of pixels. When we try to fit a model to the simulated data, the probability of a given model being the parent model from which we generated the simulated images P is given by the χ^2 distribution:

$$P \sim e^{\chi^2/2}$$

We then find the contours for 1, 2 and 3 σ by finding the level at which respectively 68, 95 and 99 percent of the cumulative distribution has a higher probability then the contour level.

6 Discussion of results

Next we will discuss the results as shown in figure 10. This is a complicated graph which needs an explanation. The axes of the subplots are those of the free parameters in the model. The axis running from 0 to 2 is the velocity, the other is the angle of rotation in degrees. This is the same space of parameters that is used in fig 9. So to see the χ^2-map of a pair of images in figure 9, look at the same location in figure 10. This location is also indicated on the subplot with a cross, as it is where the minimum χ^2 should lie. The colours on figure 10 indicate the value of χ^2. They run from 0 (black) to 10 (yellow). The contours of the probability distribution are shown in black; the solid line being 1 σ, the dashed line 2 σ and the dotted line 3 σ.
There are several reasons why the contours should be better than is shown here. As already mentioned, noise should be dependent on the flux. Outlying data points have a lower flux, but also a higher velocity and should give relatively more information on the rotation velocity of the object. In that sense we suppress the more important data by having constant noise.
The χ^2-test is suitable for independent data points, while our data actually has a correlation. Taking this into account would also improve the margins of error. The reason that we *know* the errors are not as big as they seem, is that all true minima are found at the location of the crosses, while there should be a spread around them. The most important thing we can see from these results is the double minimum that we have in most cases. Having a velocity that increases linearly with distance from the centre of the system, makes the otherwise circular object look like an ellipse at some angle on the PN.S images. This means

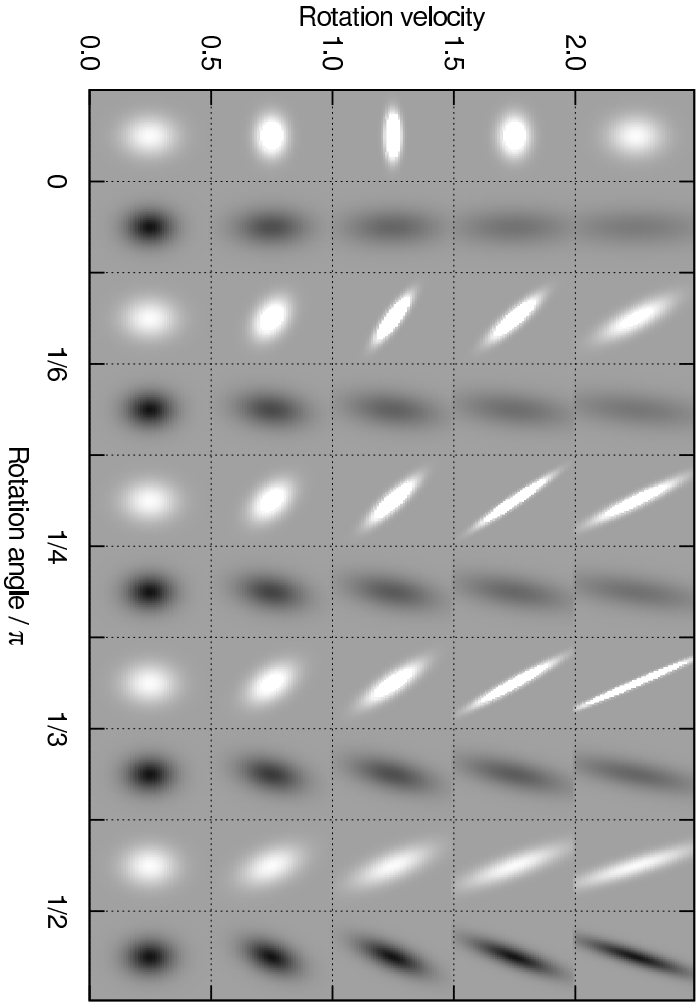

Figure 9: Left- and right-dispersed images (respectively white and black) of the 25 different models. Of course the models with no rotation all look the same.

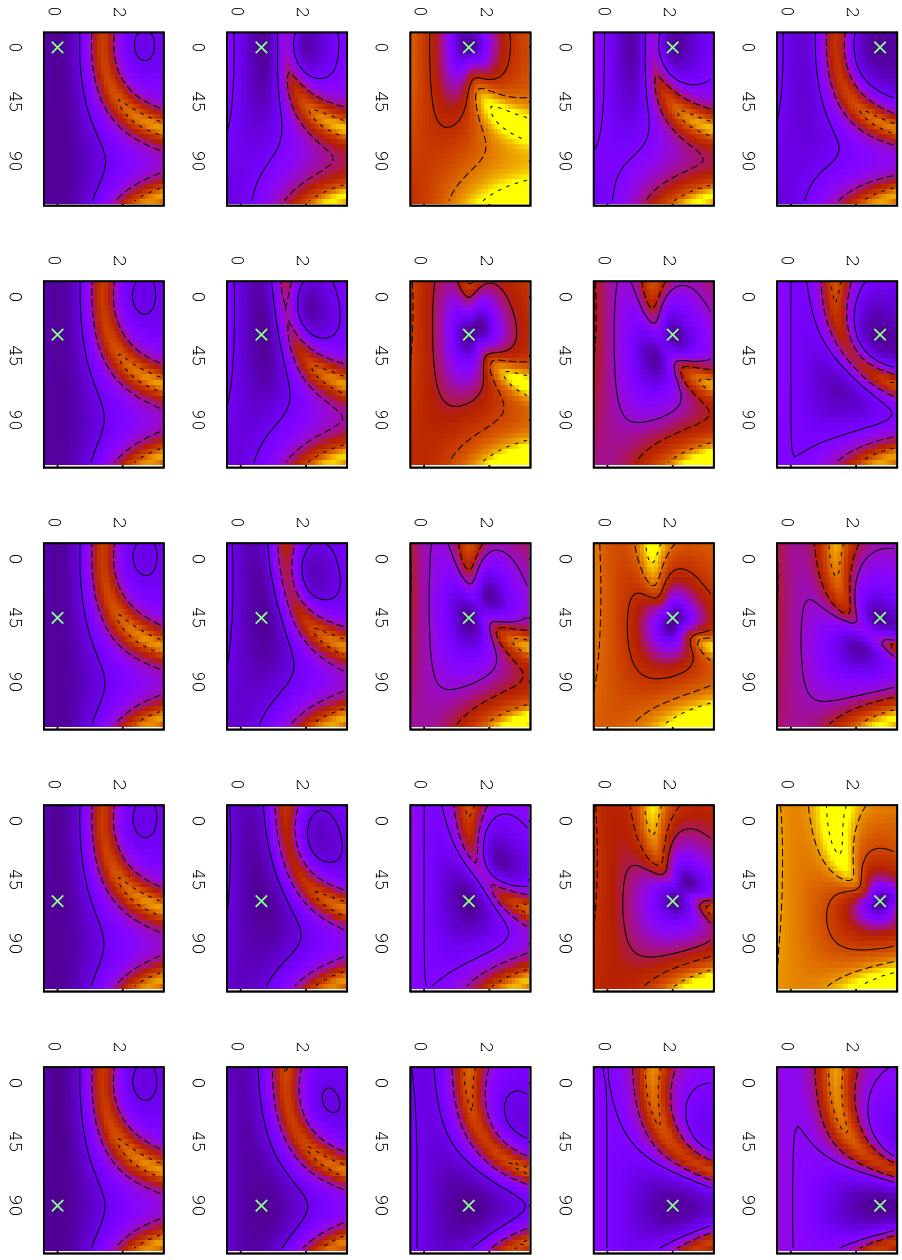

Figure 10: χ^2-map of the 25 different models. The minimum of each map should lie approximately at the position which it occupies on the total plot (marked with a cross). The contours of 1 (solid), 2 and 3 σ are plotted. The axes span the parameter space of velocity and angle.

having some velocity there is an intrinsic angle at which the projection amplifies the intensity instead of blurring it, as the projection does in the other cases. This effect can also be seen in figure 9.
Also notice that while there is a degeneracy in velocity using the simple model, on the whole the precision is better than that of the rotation angle.

7 Application on real data

7.1 Proposal by Nicola Napolitano

Napolitano has worked on a proposal to observe a galaxy cluster with the PN.S to verify the Tully-Fisher relation. He uses a few suggestive examples of galaxies near NGC 821. In most cases however this would not be so easy. The model would need to be enhanced to cover projection effects, more realistic profiles and rotation curves, which could in turn potentially introduce new degeneracies. We can still try to apply the model from this project to these objects.

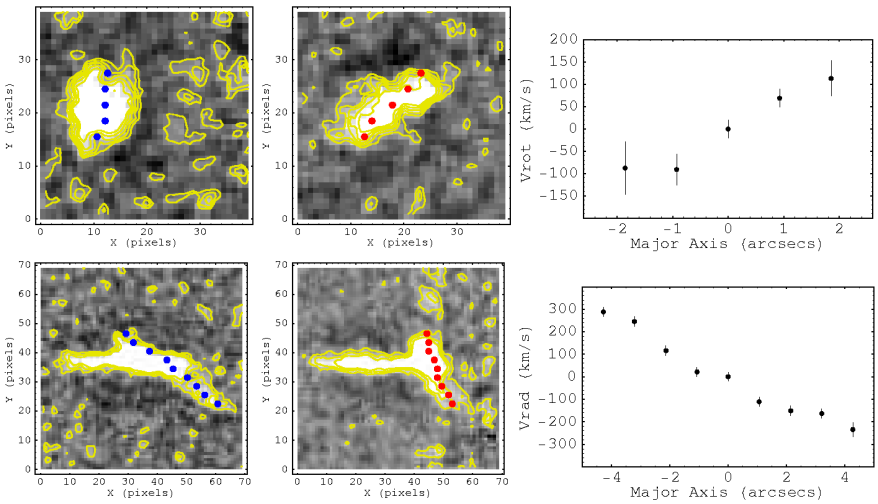

Figure 11: Examples from the observing proposal by Napolitano. These images are very nice in suggesting a way to measure a rotation curve of these galaxies. This method of determining the radial velocity would seem too naive given the results from the previous section.

We tried to fit the complete model, that is including radius, ellipticity and luminosity to some of the best objects from the NGC 821 image.

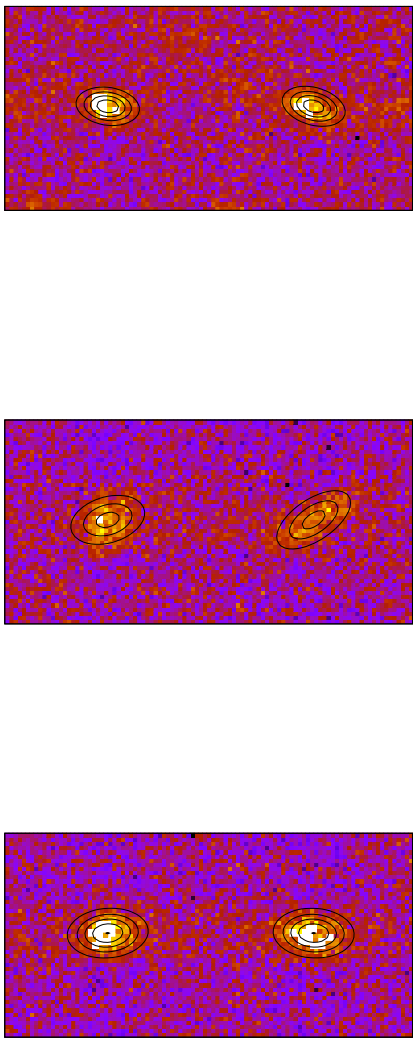

Figure 12: Median subtracted objects from the NGC 821 image. The fitted model is drawn in contours. The fits look ok, except for the middle one, which probably has a double line structure.

8 Conclusion

Complete deconvolution of the PN.S images is impossible. However if we make some assumptions about the shape of the object, we can retrieve information on the rotation velocity of the object. However, even using a very simple model some degeneracies remain. This would threaten any attempt at using PN.S data to do serious research on high redshift galaxies.

8.1 Extension

The techniques used in this project can be extended to any number of projections. If the PN.S were rotated on its mount between several exposures, a full data-cube could be reduced from the data. It is interesting in it self to see how this technique would perform against Fabry-Perot spectroscopy. Even two extra images using the PN.S (one more shot) could really improve the results using least squares fitting.

References

[1] Aaron J. Romanowsky, Nigel G. Douglas, Magda Arnaboldi, Konrad Kuijken, Michael R. Merrifield, Nicola R. Napolitano, Massimo Capaccioli, Kenneth C. Freeman - Science 301, 1696 (2003) - A Dearth of Dark Matter in Ordinary Elliptical Galaxies

[2] A. Dekel, F. Stoehr, G. A. Mamon, T. J. Cox, G.S. Novak, J. R. Primack - Nature, 437, 707 (2005) - Lost and found dark matter in elliptical galaxies

[3] N.G. Douglas, N.R. Napolitano, A. J. Romanowski, L. Coccato, K. Kuijken, M. R. Merrifield, M. Arnaboldi, O. Gerhard, K. C. Freeman, H. R. Merrett, E. Noordermeer, M. Capaccioli - ApJ, 664:257-276 (2007) - The PN.S elliptical galaxy survey: data reduction, planetary nebula catalog and basic dynamics for NGC 3379

[4] N. Napolitano - observing proposal

A Functions used to do LSF.

To do least square fitting, we need the first and second derivatives of the model. The source functions are all gaussians.
We have a function

$$F(x,y,\lambda;r,q,s,\phi,\sigma) = \frac{1}{(2\pi)^{3/2}r^2\sigma}\exp\left[-\frac{1}{2r^2}\left(u^2q+\frac{v^2}{q}\right)-\frac{1}{2\sigma^2}(s\ u-\lambda)^2\right]$$

where $u = x\cos\phi - y\sin\phi$ and $v = x\sin\phi + y\cos\phi$. Make the substitution

$$\xi \equiv (u^2q + v^2/q).$$

Some shorthands:

$$\frac{\partial u}{\partial \phi} = -v$$

$$\frac{\partial v}{\partial \phi} = u$$

$$\frac{\partial uv}{\partial \phi} = u^2 - v^2$$

$$\frac{\partial \xi}{\partial \phi} = -2uv\left(q-\frac{1}{q}\right)$$

$$\frac{\partial \xi}{\partial q} = u^2 - \frac{v^2}{q^2}$$

Then first derivatives are:

$$\frac{\partial F}{\partial r} = -\left(\frac{2}{r}-\frac{\xi}{r^3}\right)F \equiv AF$$

$$\frac{\partial F}{\partial q} = -\frac{1}{2r^2}\left(u^2-\frac{v^2}{q^2}\right)F \equiv BF$$

$$\frac{\partial F}{\partial s} = \frac{u}{\sigma^2}(\lambda - s\ u)F \equiv CF$$

$$\frac{\partial F}{\partial \phi} = \left(\frac{uv}{r^2}\left(q-\frac{1}{q}\right)+\frac{vs}{\sigma^2}(s\ u-\lambda)\right)F \equiv DF$$

Second derivatives:

$$\frac{\partial^2 F}{\partial^2 r} = A^2F + \frac{\partial A}{\partial r}F = \left(A^2 + \frac{2}{r^2} - \frac{3\xi}{r^4}\right)F$$

$$\frac{\partial^2 F}{\partial q \partial r} = ABF + \frac{\partial A}{\partial q}F = \left(AB + \frac{1}{r^3}\left(u^2 - \frac{v^2}{q^2}\right)\right)F$$

$$\frac{\partial^2 F}{\partial s \partial r} = ACF + \frac{\partial A}{\partial s}F = ACF$$

$$\frac{\partial^2 F}{\partial \phi \partial r} = ADF + \frac{\partial A}{\partial \phi}F = \left(AD - \frac{2uv}{r^3}\left(q - \frac{1}{q}\right)\right)F$$

$$\frac{\partial^2 F}{\partial r \partial q} = BAF + \frac{\partial B}{\partial r}F = \left(BA + \frac{1}{r^3}\left(u^2 - \frac{v^2}{q^2}\right)\right)F$$

$$\frac{\partial^2 F}{\partial^2 q} = B^2F + \frac{\partial B}{\partial q}F = \left(B^2 - \frac{v^2}{r^2 q^3}\right)F$$

$$\frac{\partial^2 F}{\partial s \partial q} = BCF + \frac{\partial B}{\partial s}F = BCF$$

$$\frac{\partial^2 F}{\partial \phi \partial q} = BDF + \frac{\partial B}{\partial \phi}F = \left(BD + \frac{uv}{r^2}\left(1 + \frac{1}{q^2}\right)\right)F$$

$$\frac{\partial^2 F}{\partial r \partial s} = CAF + \frac{\partial C}{\partial r}F = CAF$$

$$\frac{\partial^2 F}{\partial q \partial s} = CBF + \frac{\partial C}{\partial q}F = CBF$$

$$\frac{\partial^2 F}{\partial^2 s} = C^2F + \frac{\partial C}{\partial s}F = \left(C^2 - \frac{u^2}{\sigma^2}\right)F$$

$$\frac{\partial^2 F}{\partial \phi \partial s} = CDF + \frac{\partial C}{\partial \phi}F = \left(CD + \frac{v}{\sigma^2}\left(2us - \lambda\right)\right)F$$

$$\frac{\partial^2 F}{\partial r \partial \phi} = DAF + \frac{\partial D}{\partial r}F = \left(DA - \frac{2uv}{r^3}\left(q - \frac{1}{q}\right)\right)F$$

$$\frac{\partial^2 F}{\partial q \partial \phi} = DBF + \frac{\partial D}{\partial q}F = \left(DB + \frac{uv}{r^2}\left(1 + \frac{1}{q^2}\right)\right)F$$

$$\frac{\partial^2 F}{\partial s \partial \phi} = DCF + \frac{\partial D}{\partial s}F = \left(DC + \frac{v}{\sigma^2}(2us - \lambda)\right)F$$

$$\frac{\partial^2 F}{\partial^2 \phi} = D^2F + \frac{\partial D}{\partial \phi}F = \left(D^2 + (u^2 - v^2)\left(\frac{1}{r^2}\left(q - \frac{1}{q}\right) + \frac{s^2}{\sigma^2}\right) - u\frac{s\lambda}{\sigma^2}\right)F$$